Ultracompact hybrid stars consistent with multimessenger astrophysics

Jia Jie Li,[1] Armen Sedrakian,[2,3] and Mark Alford[4]

[1]*School of Physical Science and Technology, Southwest University, Chongqing 400715, China*
[2]*Frankfurt Institute for Advanced Studies, D-60438 Frankfurt am Main, Germany*
[3]*Institute of Theoretical Physics, University of Wrocław, 50-204 Wrocław, Poland*
[4]*Department of Physics, Washington University, St. Louis, Missouri 63130, USA*

(Received 20 July 2022; accepted 9 January 2023; published 23 January 2023)

In this work, we consider the consequences of phase transition in dense QCD on the properties of compact stars and implications for the observational program in gravitational wave and x-ray astrophysics. The key underlying assumption of our modeling is a strong first-order phase transition past the point where the hadronic branch of compact stars reaches the two-solar mass limit. Our analysis predicts ultracompact stars with very small radii—in the range of 6–9 km—living on compact star sequences that are entirely consistent with the current multimessenger data. We show that sequences featuring two-solar mass hadronic stars consistent with radio-pulsar observations are also consistent with the inferences of large radii for massive neutron stars by NICER x-ray observations of neutron stars and the small radii predicted by gravitational waves analysis of the binary neutron star inspiral event GW170817 for our models that feature a strong first-order QCD phase transition.

DOI: 10.1103/PhysRevD.107.023018

I. INTRODUCTION

There has been significant progress in the search for the ultimate state of extremely dense (by an order of magnitude larger than in the ordinary nuclei) matter over the past decade due to new astrophysical observations of compact stars (CS). These include the GW170817 event involving a merger of two compact stars which heralded the beginning of the multimessenger era of exploration of compact stars [1–3], the x-ray observation of nearby neutron stars by the NICER instrument [4–7], and measurement of massive radiopulsars in binaries with white dwarfs [8].

The description of ultradense matter should ultimately be based on first-principles QCD which is currently out of reach in the density-temperature range relevant for compact stars. Thus, a combination of phenomenological models with the available experimental/astrophysical data is the best option to model the properties of dense, strongly interacting states of matter; for reviews, see Refs. [9,10]. A likely outcome of the compression of the nucleonic matter is a phase transition to the liberated quark phase, as envisioned already several decades ago [11–13] and extensively studied over the past decades. It has been realized that a first-order phase transition between the hadronic and quark phase may lead to a new branch of stable hybrid stars —stars featuring a dense quark core enveloped by nucleonic matter. One interesting feature of hybrid CS is the existence of *twin configurations*: two stars with different radii but the same masses, the larger one being purely nucleonic and the more compact one being a hybrid star. These hybrid stars comprise the *third family of compact stars* after white dwarfs and neutron stars [14–26]. Below we will use the specific constant speed of sound parametrization of the quark phase [27,28], but qualitatively similar results are expected for alternative models, for example, multpolytropic equation of state (EOS) [21]. Indeed, modeling based on the constant sound speed (CSS) and multipolytropic EOS leads to qualitatively similar results; see Ref. [29].

Here we address the structure of hybrid stars which are consistent with current astrophysical observations and show that a strong first-order phase transition may lead to the emergence of hybrid stars with extremely small radii and a very narrow range of masses for any given parameter set. However, the masses of these objects can be varied broadly by changing the parameters of the equation of state (EOS) while keeping the resultant stellar sequences consistent with current multimessenger astrophysical data. This sheds new light on the ways the current astrophysical constraints can be interpreted. For example, our analysis below confirms that, as previously noted [24,26], the masses and radii inferred from NICER observations can be interpreted as originating from the nucleonic branch of mass twins, while the hybrid branch contains stars whose tidal deformabilities (hereafter TD) are consistent with the GW170817 observation. Another implication of our study is a shift in the paradigm stating that small $R \simeq 6$–9 km radius objects, if discovered, would be strange stars (for a review see Ref. [30]). As we show below, ultracompact objects arising from a strong first-order phase transition can have radii covering the range where so far only strange stars

(objects arising within the Witten-Bodmer conjecture about the ground state of absolute stable state of matter [31,32]) were predicted. Previously, Drago *et al.* [33] addressed the compatibility of large masses and small radii, in terms of two separate families of compact stars. Their scenario invokes very compact hadronic stars, whose EOS is soft, and strange stars whose EOS is stiff. The strange star hypothesis by itself is compatible with the NICER data [34] and deformabilities inferred from GW170817 [35], but has been the only one that accounted for very small radii in the range of 6–9 km. As we show below, large masses and small radii are possible to accommodate within a single-family scenario, which needs to be incorporated in the analysis of the current astrophysics data.

II. CONSTRUCTING THE EQUATION OF STATE

To model the EOS of low-density hadronic matter we use the covariant density functional (CDF) approach based on the Lagrangian of stellar matter with baryonic degrees of freedom $\mathcal{L} = \mathcal{L}_b + \mathcal{L}_m + \mathcal{L}_l + \mathcal{L}_{\rm em}$, where the baryon Lagrangian is given by

$$\mathcal{L}_b = \sum_b \bar{\psi}_b [\gamma^\mu (i\partial_\mu - g_{\omega b}\omega_\mu - g_{\rho b}\tau\cdot\rho_\mu) - (m_b - g_{\sigma b}\sigma)]\psi_b, \tag{1}$$

with the b sum running over the $J^P = \frac{1}{2}^+$ baryon octet in general, but we restrict the discussion to nucleons only; ψ_b are the nucleonic Dirac fields with masses m_b, and σ, ω_μ, and $\boldsymbol{\rho}_\mu$ are the mesonic fields which mediate the interaction among baryon fields. The remaining pieces of the Lagrangian correspond to the mesonic, leptonic, and electromagnetic contributions, respectively. These are standard and are given, e.g., in Ref. [36]. The density-dependent nucleon-meson couplings g_{mb} are fixed at saturation density at the values prescribed by the DDME2 parametrization [37]. Their density dependence differs from that parametrization and is varied to match the resulting EOS with the phenomenological expansion of the energy density of nuclear matter [38–40],

$$E(\chi,\delta) \simeq E_{\rm sat} + \frac{1}{2!}K_{\rm sat}\chi^2 + \frac{1}{3!}Q_{\rm sat}\chi^3 + E_{\rm sym}\delta^2 + L_{\rm sym}\delta^2\chi + \mathcal{O}(\chi^4,\chi^2\delta^2), \tag{2}$$

where $\chi \equiv (\rho - \rho_{\rm sat})/3\rho_{\rm sat}$, $\rho_{\rm sat}$ is the saturation density, and $\delta = (\rho_{\rm n} - \rho_{\rm p})/\rho$ is the isospin asymmetry with $\rho_{\rm n(p)}$ being the neutron(proton) number densities. The coefficients in this double expansion are referred to commonly as the incompressibility $K_{\rm sat}$, skewness $Q_{\rm sat}$, symmetry energy $E_{\rm sym}$, and its slope $L_{\rm sym}$. The mapping between the CDF and the phenomenological expansion (2) allows us to express the gross properties of compact stars in terms of physically transparent quantities.

In this work, we study a family of representative nucleonic EOSs obtained by varying $L_{\rm sym}$ and $Q_{\rm sat}$ at fixed values of $E_{\rm sym}(\rho_c) = 27.09$ MeV ($\rho_c = 0.11$ fm^{-3}) and $K_{\rm sat} = 251.15$ MeV [39]. The parameter $Q_{\rm sat}$ controls the high-density behavior of the EOS, and thus, the maximum mass of a static nucleonic CS, whereas $L_{\rm sym}$ controls the intermediate-density EOS and is strongly correlated with the radius of the nucleonic stars. We consider values of the slope parameter in the range $45 \le L_{\rm sym} \le 105$ MeV. The upper limit of $L_{\rm sym}$ is the central value of the PREX-II measurement interpretation by Refs. [41,42]; the lower bound corresponds to the one derived from the analysis of the same experimental data in Ref. [43]. The values for skewness are less constrained and we use values $Q_{\rm sat} = 300$ and 900 MeV which predict maximal masses of nucleonic sequences within the mass range $2.30 \le M_{\rm max}/M_\odot \le 2.55$. This mass range allows for the nucleonic CS branch to account for the measured lower bound on the maximum mass $M/M_\odot = 2.08 \pm 0.07$ [44]. The pairs of $Q_{\rm sat}$ and $L_{\rm sym}$ values bracket the range of accepted values of these parameters. Our analysis shows that qualitatively similar results are obtained when using other pairs of these parameters that are drawn from the bracketed range. The parameters for four nucleonic EOS models are listed in Table I.

The EOS of the quark phase is modeled by a CSS parametrization [27,28] which offers a *synthetic* model motivated by microscopic computations [20], i.e.,

$$p(\varepsilon) = \begin{cases} p_{\rm tran}, & \varepsilon_{\rm tran} < \varepsilon < \varepsilon_{\rm tran} + \Delta\varepsilon, \\ p_{\rm tran} + s[\varepsilon - (\varepsilon_{\rm tran} + \Delta\varepsilon)], & \varepsilon_{\rm tran} + \Delta\varepsilon < \varepsilon, \end{cases} \tag{3}$$

TABLE I. The meson masses and the meson-nucleon coupling constants at the nuclear saturation density (column I), the constants determining the density dependence of the meson-nucleon couplings for $Q_{\rm sat} = 300$ (column II) and 900 MeV (column III). The last two rows of columns II and III list the couplings that produce $L_{\rm sym} = 45$ (left entry) and 105 MeV (right entry).

		$Q_{\rm sat}$	300	900
	I		II	III
m_σ	550.1238	a_σ	1.3690	1.4730
m_ω	783.0000	b_σ	0.8555	1.9201
m_ρ	763.0000	c_σ	1.3353	3.0965
g_σ	10.5396	d_σ	0.4996	0.3281
g_ω	13.0189	a_ω	1.3752	1.4571
		b_ω	0.7205	1.6107
		c_ω	1.1493	2.5947
		d_ω	0.5385	0.3584
		g_ρ	3.3379/4.2193	3.3253/4.2111
		a_ρ	0.6442/0.0506	0.6552/0.0569

where $p_{\rm tran}$ and $\varepsilon_{\rm tran}$ are the pressure and energy density at which the transition from hadronic (hereafter H) to high-density quark phase (hereafter Q) takes place; s is the squared speed of sound (in natural units) in the quark matter phase and $\Delta\varepsilon$ is the discontinuity in energy density; note that there is no state with energy between $\varepsilon_{\rm tran}$ and $\varepsilon_{\rm tran}+\Delta\varepsilon$. This parametrization agrees with the predictions of computations based on the Nambu–Jona-Lasinio model supplemented by vector repulsion [45–48]. In constructing our models we will use the Maxwell construction to match our nucleonic EOS to the quark one (3).

III. THE MASS-RADIUS DIAGRAM AND TIDAL DEFORMABILITIES

The three quark matter parameters ($p_{\rm tran}$, $\Delta\varepsilon$, s) fully determine the mass-radius (hereafter $M-R$) curves for hybrid stars for any given nucleonic EOS. It is convenient for further discussion to denote maximum/minimum masses for the branches by $M^{\rm H}_{\rm max}$, $M^{\rm Q}_{\rm max}$, and $M^{\rm Q}_{\rm min}$. See Fig. 1 for an illustration of these parameters and the features of the $M-R$ diagram, in particular the maxima and minima that may arise. Note that the branch extending up to $M^{\rm Q}_{\rm max}$ corresponds to the third family.

Figure 1 shows the scenario under consideration in which the phase transition occurs at a high enough density, $\rho_{\rm tran}/\rho_{\rm sat}\gtrsim 3.0$, so that the heaviest star on the hadronic branch has a mass of $2M_\odot$. In this case, the hybrid branches lie at lower masses and are nearly flat. In the same figure, we contrast this scenario with the one studied in the light of multimessenger data in Refs. [21,24], in which the phase transition occurs at a lower density, $\rho_{\rm tran}/\rho_{\rm sat}\lesssim 2.0$, causing the hadronic branch to end at a lower mass, $M^{\rm H}_{\rm min}=1.3M_\odot$, and the hybrid branch extends up to $M^{\rm Q}_{\rm max}>2M_\odot$. Our sequences can be confronted with current astrophysical observational constraints shown also in Fig. 1 which include: (a) the ellipses indicating the regions of $M-R$ diagram compatible with the analysis of NICER observations of PSR J0030 + 0451 and J0740 + 6620 [4–7]; (b) the regions of $M-R$ diagram that are compatible with the parameters of the two compact stars that merged in the gravitational wave event GW170817 [2]. For both observations, the ellipses show the 90% credible intervals (CIs). Note that ellipses referring to GW170817 have been obtained under the assumption of a hadronic star, therefore they are relevant, strictly speaking, only for constraining the hadronic branches on the $M-R$ diagram. Figure 1 shows, in addition, the sensitivity of results to varying the quark matter speed of sound squared s. We see that choosing the maximum value $s=1.0$ yields the widest range of masses on the hybrid branch and hence for twin stars.

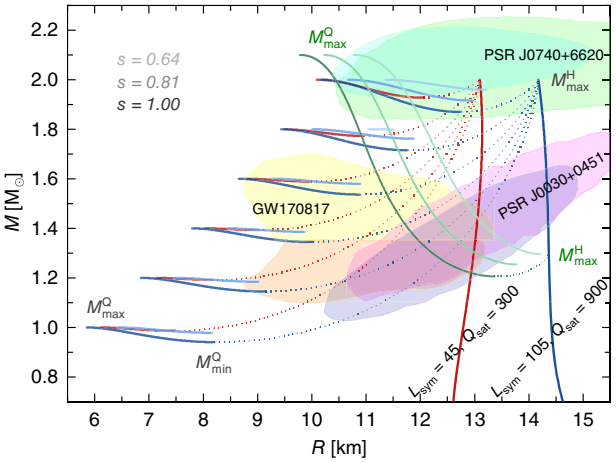

FIG. 1. $M-R$ relation for hybrid EOS models with a phase transition at high density for stiff-stiff nucleonic EOSs with $L_{\rm sym}=105$, $Q_{\rm sat}=900$ MeV, and soft-soft one with $L_{\rm sym}=45$, $Q_{\rm sat}=300$ MeV. The sequences of stars are constructed from a nucleonic model by fixing $M^{\rm H}_{\rm max}/M_\odot=2.0$ on the nucleonic branch, while varying the $M^{\rm Q}_{\rm max}/M_\odot$ in the range 1.0–2.0 and the speed of sound squared s. For comparison, we also show the sequences in the case of low-maximum hadronic mass $M^{\rm H}_{\rm max}/M_\odot=1.3$, studied previously in Refs. [21,24], for the same speeds of sound. Note that GW170817 ellipses assume a hadronic EOS and constrain only the hadronic branches of the stellar sequences.

In Fig. 2 we fix the maximum mass of the nucleonic branch $M^{\rm H}_{\rm max}=2.0M_\odot$ and squared sound of speed $s=1.0$ and then vary $M^{\rm Q}_{\rm max}/M_\odot$ from 1.0 to 2.0 to show the range covered in the $M-R$ diagram by these types of sequences.

To assess the range of variations in the sequences arising from the uncertainties in the *nucleonic sector* we consider nucleonic EOSs with $L_{\rm sym}$ taking values 45,105 MeV and $Q_{\rm sat}$ taking values 300,900 MeV. The value of $L_{\rm sym}$ controls the intermediate density and $Q_{\rm sat}$ the high-density behavior on the nucleonic branch; see Figs. 1 and 2. So in Fig. 2 we have $(L_{\rm sym},Q_{\rm sat})=(105,300)$ MeV corresponding to a

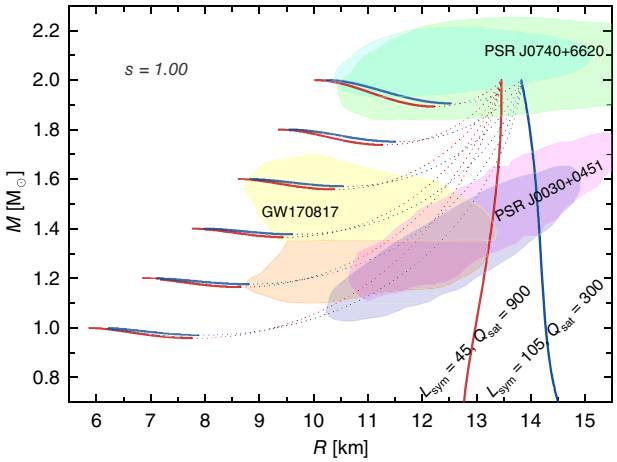

FIG. 2. $M-R$ relation for hybrid EOS models featuring high density phase transition with two examples of nucleonic EOSs, specifically the soft-stiff one with $L_{\rm sym}=45$, $Q_{\rm sat}=900$ MeV and stiff-soft one $L_{\rm sym}=105$, $Q_{\rm sat}=300$ MeV. The value of sound speed squared is fixed at $s=1.0$.

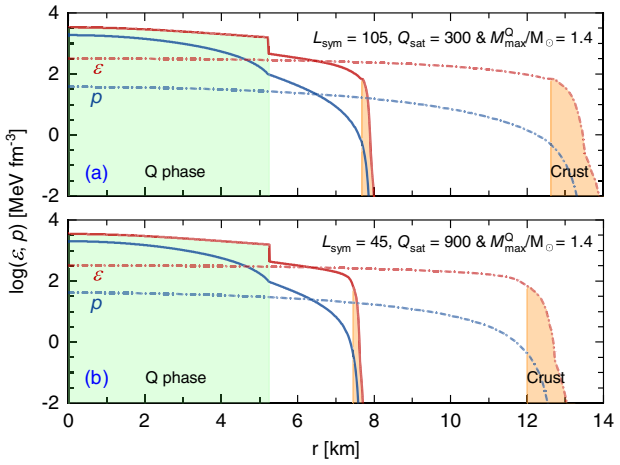

FIG. 3. Radial profiles of energy density and pressure (on a logarithmic scale) for twin stars with masses $M = M^Q_{\max} = 1.40M_\odot$. The results for purely nucleonic stars are shown by dotted, and those for hybrid stars are shown by solid lines. Two nucleonic EOSs have been used: a soft-stiff one with $L_{\rm sym} = 45$, $Q_{\rm sat} = 900$ MeV and a stiff-soft one with $L_{\rm sym} = 105$, $Q_{\rm sat} = 300$ MeV. The quark core and crust regions are shaded for clarity.

"stiff-soft" (intermediate-density stiff and high-density soft) hadronic EOS and $(L_{\rm sym}, Q_{\rm sat}) = (45, 900)$ MeV for the inverse "soft-stiff" EOS.

Figure 3 shows the internal structure of twin stars with masses $M = 1.40M_\odot$ by plotting the energy density and pressure as a function of distance from the center for purely nucleonic (dotted lines) and hybrid (solid lines) stars. The highly compact hybrid configurations have an appearance that is similar to frequently studied less compact hybrid stars. As seen in Fig. 3 there is a moderate-size quark core of about 5 km, a nucleonic layer of neutron-proton-electron fluid of about 2 km, and a thin crust of several 100 m. Clearly, these objects do not resemble a strange star that is largely composed of quark matter core with a thin crust floating on top of it, due to support provided by Coulomb forces [30].

As seen from Figs. 1 and 2, all nucleonic branches are fully compatible with the masses and radii inferred by the NICER instrument for both parameter sets corresponding to stiff-soft(stiff) and soft-stiff(soft) nucleonic EOSs.

There is no tension between the NICER inferences and the soft EOS needed to account for GW170817 analysis, as implied by statistical models [49–52], including those which allow for first-order phase transitions [53–55]. There is also no evidence for the need for strong first-order phase transition in the analysis of statistical models, while some of them disfavor such transition [55]. The large value of $L_{\rm sym}$ suggested by an analysis [42] of the PREX-II experiment (but see also Ref. [43]) requires a hard nucleonic EOS which becomes consistent with the GW170817 event in the case of the H-Q phase transition [24,26]. For an alternative

TABLE II. Parameters of the used EOS with a fixed maximum mass of the hadronic branch $M^{\rm H}_{\max} = 2.0M_\odot$ and speed of sound squared $s = 1.0$ in quark matter. The maximum masses of ultracompact hybrid stars are shown in the range $M^{\rm Q}_{\max}/M_\odot = 1.00$–$1.60$ with a step of 0.20. The remaining columns specify the corresponding values of $Q_{\rm sat}$, $L_{\rm sym}$, and $\varepsilon_{\rm tran}$ and $\Delta\varepsilon/\varepsilon_{\rm tran}$. The last column shows the range of masses within which twin ultracompact stars exist.

$Q_{\rm sat}$	$L_{\rm sym}$	$\varepsilon_{\rm tran}$	$M^{\rm Q}_{\max}$	$\Delta\varepsilon/\varepsilon_{\rm tran}$	$\Delta M_{\rm twin}$
300	45	487.132	1.00	5.0604	0.0133
			1.20	3.3866	0.0077
			1.40	2.3407	0.0065
			1.60	1.6325	0.0109
300	105	463.315	1.00	5.2178	0.0283
			1.20	3.4885	0.0232
			1.40	2.4100	0.0223
			1.60	1.6856	0.0288
900	45	433.640	1.00	5.5915	0.0411
			1.20	3.7446	0.0350
			1.40	2.6015	0.0341
			1.60	1.8358	0.0412
900	105	414.476	1.00	5.7823	0.0595
			1.20	3.8663	0.0547
			1.40	2.6857	0.0551
			1.60	1.8988	0.0635

which used nonparametric EOSs and constrains the symmetry energy and its slope directly from observations with minimal modeling assumptions, see Ref. [56].

The range of masses of such stars can be remarkably broad when varying the EOS (not the central pressure) and covering the interval $1.0 \le M/M_\odot \le 2.0$. Thus, a consequence of high-density QCD phase transition is the existence of ultracompact stars—a prediction that is consistent with the astrophysical constraints obtained to date. The parameters fully characterizing the hybrid EOS models which produce ultracompact stars are given in Table II. We note that the only other models that predict such small radii that may be consistent with the current observational data are those based on the idea of strange stars [30].

As demonstrated by multiple analyses of the GW170817 event, the TDs provide excellent diagnostics of the gross properties of neutron stars. Note that TDs provide information on the cold EOSs of dense matter, as they are probes originating from the premerger phase of binary inspiral. Figure 4 compares our theoretical TDs for hybrid stars with the observational constraints for this quantity obtained from the analysis of the GW170817 event [2]. Our comparison adopts the chirp mass as $\mathcal{M} = 1.186M_\odot$ and utilizes only the analysis which assumes the (more plausible) low-spin case [2]. The masses of the members of the binary in the GW170817 are found to be in the range $1.16 - 1.60M_\odot$ at 90% CI. To obtain the TDs we (a) fix the values of $L_{\rm sym}$ and $Q_{\rm sat}$ which selects the nuclear EOS; (b) choose

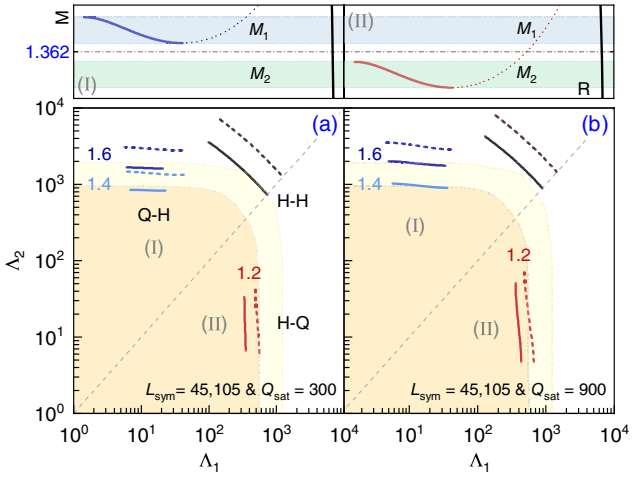

FIG. 4. Dimensionless TD of compact objects for a fixed value of binary chirp mass $\mathcal{M}/M_\odot = 1.186$. The shaded regions correspond to the 50% and 90% CIs taken from the analysis of the GW170817 event. The EOS models with strong first-order phase transition are fixed by the values $M^{\rm H}_{\rm max}/M_\odot = 2.0$ and $M^{\rm Q}_{\rm max}/M_\odot = 1.2$ (red curves), 1.4 (blue curves), 1.6 (dark blue curves), and $s = 1.0$. The type of binary components (Q/H) with mass $M_1 - M_2$ are indicated in the plot. Panel (a): soft-soft and stiff-soft hadronic EOS results are shown by solid and dashed lines; panel (b): soft-stiff and stiff-stiff hadronic EOSs are shown by solid and dashed lines. The upper left inset shows a schematic $M - R$ diagram for the cases $M^{\rm Q}_{\rm max}/M_\odot = 1.4$, 1.6, where the binary is of the Q-H type and the hybrid branch lies above the average value $M/M_\odot = 1.362$. The right inset shows the same for $M^{\rm Q}_{\rm max}/M_\odot = 1.2$, in which case the binary is of the H-Q type with the hybrid branch lying below the average value $M/M_\odot = 1.362$. These two cases are marked in the plots and insets by Latin numerals I and II, respectively.

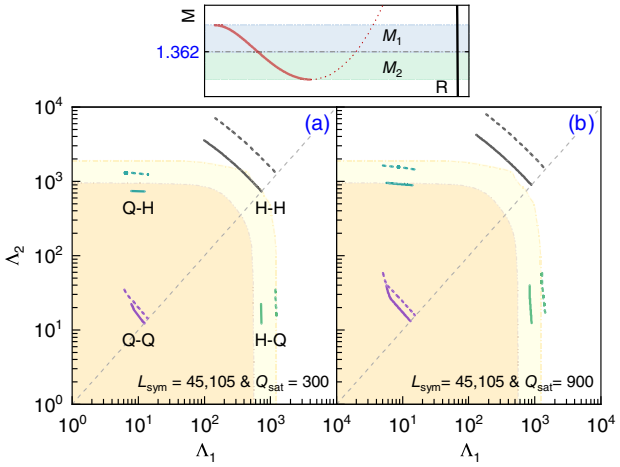

FIG. 5. Dimensionless TD for the case of EOSs with the hybrid branch covering a range of masses around the average value $M/M_\odot = 1.362$ as illustrated in the upper inset showing the $M - R$ relation. The remaining parameters are chosen as in Fig. 4. There are four types of binaries composed of hadronic (H) and/or hybrid (Q) stars. Panel (a): soft-soft and stiff-soft hadronic EOS results are shown with solid and dashed lines; (b): soft-stiff and stiff-stiff hadronic EOSs are shown by solid and dashed lines.

$M^{\rm H}_{\rm max}/M_\odot = 2.0$, $M^{\rm Q}_{\rm max}/M_\odot = 1.2$, 1.4, 1.6 and $s = 1.0$ which fixes three hybrid EOSs each corresponding to a value of $M^{\rm Q}_{\rm max}/M_\odot$.

Figure 4 shows the mutual dependence of TDs $\Lambda_1 - \Lambda_2$ of members of a binary for three choices of $M^{\rm Q}_{\rm max}/M_\odot$. The shaded areas correspond to the 50% and 90% CIs as indicated in the plot (we adopt the results obtained from the PhenomPNRT waveform model [3]). Note that the diagonal on this plot corresponds to the case of an equal-mass binary with $M_{1,2} = 1.362M_\odot$. As seen, the case of the H-H binary generates $\Lambda_1 - \Lambda_2$ values at the boundary or outside of the 90% CI region for any choice of the stiffness of the EOS. In the case of $M^{\rm Q}_{\rm max}/M_\odot = 1.4$ and 1.6 the mass range of the hybrid branch is above the average value $M/M_\odot = 1.362$ (as indicated in the left inset showing $M - R$ diagram). In the case $M^{\rm Q}_{\rm max}/M_\odot = 1.2$ the opposite is the case, i.e., the hybrid branch is below this value, see the right inset. As a consequence, the $\Lambda_1 - \Lambda_2$ tracks in the first case are in the upper half of the plot (Q-H binaries). In the second case, they are in the lower half of the plot (H-Q binaries). These models are compatible with the range determined for GW170817 for soft-soft, stiff-soft (panel a) and soft-stiff, stiff-stiff (panel b) EOSs. An exception is the case $M^{\rm Q}_{\rm max}/M_\odot = 1.6$ when the intermediate-density EOS is chosen to be stiff. From the analysis above, one may conclude that the observations can be explained by appropriate choices of nuclear and quark EOSs.

Figure 5 shows the same as in Fig. 4, but in this case, where the quark matter EOS is chosen so that the hybrid branch covers a range of masses whose average value is $1.362M_\odot$, see the inset. Each member of the binary can be chosen from either of H or Q branches, so four combinations of stars are possible. It is seen that all the pairs lie within the allowed range except the H-H pair which is at the boundary or outside of 90% CI. Interestingly, the nucleonic EOSs of hybrid stars need not be soft. Even with an EOS that is stiff at intermediate densities (stiff-stiff or stiff-soft EOS), a Q-Q binary, consisting of two ultracompact hybrid stars with very small radii can have a combined TD as low as $\tilde{\Lambda}_{1.186} \simeq 10$. This suggests that the multimessenger data can be accounted for if PSR J0740 + 6620 and J0030 + 0451 are purely nucleonic stars, whereas the two components of the GW170817 binary are ultracompact hybrid stars.

IV. CONCLUSIONS

To summarize, we have uncovered several implications of the strongly first-order phase transitions at high density in the QCD phase diagram that are of fundamental importance for the analysis of the data from current and future gravitational-wave observatories, x-ray missions and

terrestrial experiments aimed at the determination of the skin of nuclei. First, we have confirmed that the nuclear EOS does not need to be soft to account for the GW170817 event, as the phase transitions allow for the emergence of hybrid stars with properties consistent with the GW170817 analysis [24,26]. The NICER inferences are accounted for by invoking pure nucleonic stars that live on the hadronic (second family) branch of compact stars and consistency with an analysis of the PREX-II is achieved (which was precluded in models without phase transition). Second, we determine the range of the masses for which twin configurations, i.e., identical-mass stars with different radii, arise. This analysis shows that the priors in the statistical analysis of the data should be constructed consistent with the possibility of a first-order phase transition with star masses in a wide range $1.0 \leq M/M_{\odot} \leq 2.5$ and radii covering also the range of small radii 6–9 km which was thought to be only achievable for strange stars, and is currently excluded by the NICER analysis at 90% CI.

In our proposal, both branches of stars consist of stars with thick nucleonic crusts, consistent with observations of surface phenomena such as seismic vibrations after giant flares in magnetars [57–59], the thermal response of the crust to accretion [60,61], the contribution of the crust to the moment of inertia and glitches [62,63], etc. This provides an alternative to scenarios such as that proposed in Ref. [33] where one of the branches consists of strange/quark stars with a very thin nucleonic crust.

ACKNOWLEDGMENTS

M. A. is partly supported by the U.S. Department of Energy, Office of Science, Office of Nuclear Physics under Award No. DE-FG02-05ER41375. J. L. is supported by the National Natural Science Foundation of China (Grant No. 12105232), the Fundamental Research Funds for the Central Universities (Grant No. SWU-020021), and by the Venture and Innovation Support Program for Chongqing Overseas Returnees (Grant No. CX2021007). The research of A. S. was funded by Deutsche Forschungsgemeinschaft Grant No. SE 1836/5-2 and the Polish NCN Grant No. 2020/37/B/ST9/01937 at Wrocław University.

[1] B. P. Abbott, R. Abbott, T. D. Abbott *et al.* (LIGO Scientific, Virgo Collaborations), Phys. Rev. Lett. **119**, 161101 (2017).
[2] B. P. Abbott, R. Abbott, T. D. Abbot *et al.* (LIGO Scientific, Virgo Collaborations), Phys. Rev. Lett. **121**, 161101 (2018).
[3] B. P. Abbott, R. Abbott, T. D. Abbot *et al.* (LIGO Scientific, Virgo Collaborations), Phys. Rev. X **9**, 011001 (2019).
[4] T. E. Riley, A. L. Watts, S. Bogdanov *et al.*, Astrophys. J. Lett. **887**, L21 (2019).
[5] T. E. Riley, A. L. Watts, P. S. Ray *et al.*, Astrophys. J. Lett. **918**, L27 (2021).
[6] M. C. Miller, F. K. Lamb, A. J. Dittmann *et al.*, Astrophys. J. Lett. **887**, L24 (2019).
[7] M. C. Miller, F. K. Lamb, A. J. Dittmann *et al.*, Astrophys. J. Lett. **918**, L28 (2021).
[8] H. T. Cromartie, E. Fonseca, S. M. Ransom *et al.* (NANOGrav Collaboration), Nat. Astron. **4**, 72 (2020).
[9] M. G. Alford, A. Schmitt, K. Rajagopal, and T. Schäfer, Rev. Mod. Phys. **80**, 1455 (2008).
[10] R. Anglani, R. Casalbuoni, M. Ciminale, N. Ippolito, R. Gatto, M. Mannarelli, and M. Ruggieri, Rev. Mod. Phys. **86**, 509 (2014).
[11] D. D. Ivanenko and D. F. Kurdgelaidze, Astrophysics **1**, 251 (1965).
[12] N. Itoh, Prog. Theor. Phys. **44**, 291 (1970).
[13] J. C. Collins and M. J. Perry, Phys. Rev. Lett. **34**, 1353 (1975).
[14] U. H. Gerlach, Phys. Rev. **172**, 1325 (1968).
[15] R. L. Bowers, A. M. Gleeson, and R. D. Pedigo, Astrophys. J. **213**, 840 (1977).
[16] B. Kämpfer, J. Phys. A **14**, L471 (1981).
[17] N. K. Glendenning and C. Kettner, Astron. Astrophys. **353**, L9 (2000), https://ui.adsabs.harvard.edu/abs/2000A%26A...353L...9G/abstract.
[18] K. Schertler, C. Greiner, J. Schaffner-Bielich, and M. H. Thoma, Nucl. Phys. **A677**, 463 (2000).
[19] S. Benic, D. Blaschke, D. E. Alvarez-Castillo, T. Fischer, and S. Typel, Astron. Astrophys. **577**, A40 (2015).
[20] M. G. Alford and A. Sedrakian, Phys. Rev. Lett. **119**, 161104 (2017).
[21] D. E. Alvarez-Castillo, D. B. Blaschke, A. G. Grunfeld, and V. P. Pagura, Phys. Rev. D **99**, 063010 (2019).
[22] S. Han and A. W. Steiner, Phys. Rev. D **99**, 083014 (2019).
[23] K. Otto, M. Oertel, and B.-J. Schaefer, Phys. Rev. D **101**, 103021 (2020).
[24] J. J. Li, A. Sedrakian, and M. Alford, Phys. Rev. D **104**, L121302 (2021).
[25] J. J. Li, A. Sedrakian, and M. Alford, Phys. Rev. D **101**, 063022 (2020).
[26] J.-E. Christian and J. Schaffner-Bielich, Astrophys. J. **935**, 122 (2022).
[27] J. L. Zdunik and P. Haensel, Astron. Astrophys. **551**, A61 (2013).
[28] M. G. Alford, S. Han, and M. Prakash, Phys. Rev. D **88**, 083013 (2013).
[29] V. Paschalidis, K. Yagi, D. Alvarez-Castillo, D. B. Blaschke, and A. Sedrakian, Phys. Rev. D **97**, 084038 (2018).
[30] F. Weber, Prog. Part. Nucl. Phys. **54**, 193 (2005).
[31] E. Witten, Phys. Rev. D **30**, 272 (1984).
[32] A. R. Bodmer, Phys. Rev. D **4**, 1601 (1971).
[33] A. Drago, A. Lavagno, and G. Pagliara, Phys. Rev. D **89**, 043014 (2014).

[34] J. E. Horvath and P. H. R. S. Moraes, Int. J. Mod. Phys. D **30**, 2150016 (2021).
[35] O. Lourenço, C. H. Lenzi, M. Dutra, E. J. Ferrer, V. de la Incera, L. Paulucci, and J. E. Horvath, Phys. Rev. D **103**, 103010 (2021).
[36] A. Sedrakian, J.-J. Li, and F. Weber, arXiv:2105.14050.
[37] G. A. Lalazissis, T. Niksic, D. Vretenar, and P. Ring, Phys. Rev. C **71**, 024312 (2005).
[38] J. Margueron, R. Hoffmann Casali, and F. Gulminelli, Phys. Rev. C **97**, 025806 (2018).
[39] J. J. Li and A. Sedrakian, Phys. Rev. C **100**, 015809 (2019).
[40] B.-A. Li, B.-J. Cai, W.-J. Xie, and N.-B. Zhang, Universe **7**, 182 (2021).
[41] D. Adhikari, H. Albataineh, D. Androic *et al.* (PREX Collaboration), Phys. Rev. Lett. **126**, 172502 (2021).
[42] B. T. Reed, F. J. Fattoyev, C. J. Horowitz, and J. Piekarewicz, Phys. Rev. Lett. **126**, 172503 (2021).
[43] P.-G. Reinhard, X. Roca-Maza, and W. Nazarewicz, Phys. Rev. Lett. **127**, 232501 (2021).
[44] E. Fonseca, H. T. Cromartie, T. T. Pennucci *et al.*, Astrophys. J. Lett. **915**, L12 (2021).
[45] D. Blaschke, T. Klahn, R. Lastowiecki, and F. Sandin, J. Phys. G **37**, 094063 (2010).
[46] L. Bonanno and A. Sedrakian, Astron. Astrophys. **539**, A16 (2012).
[47] T. Klähn, R. Łastowiecki, and D. Blaschke, Phys. Rev. D **88**, 085001 (2013).
[48] A. Pfaff, H. Hansen, and F. Gulminelli, Phys. Rev. C **105**, 035802 (2022).
[49] T. Dietrich, M. W. Coughlin, P. T. H. Pang, M. Bulla, J. Heinzel, L. Issa, I. Tews, and S. Antier, Science **370**, 1450 (2020).
[50] P. Landry, R. Essick, and K. Chatziioannou, Phys. Rev. D **101**, 123007 (2020).
[51] G. Raaijmakers, S. K. Greif, K. Hebeler, T. Hinderer, S. Nissanke, A. Schwenk, T. E. Riley, A. L. Watts, J. M. Lattimer, and W. C. G. Ho, Astrophys. J. Lett. **918**, L29 (2021).
[52] B. Biswas, Astrophys. J. **921**, 63 (2021).
[53] P. T. H. Pang, T. Dietrich, I. Tews, and C. Van Den Broeck, Phys. Rev. Res. **2**, 033514 (2020).
[54] I. Legred, K. Chatziioannou, R. Essick, S. Han, and P. Landry, Phys. Rev. D **104**, 063003 (2021).
[55] P. T. H. Pang, I. Tews, M. W. Coughlin, M. Bulla, C. Van Den Broeck, and T. Dietrich, Astrophys. J. **922**, 14 (2021).
[56] R. Essick, P. Landry, A. Schwenk, and I. Tews, Phys. Rev. C **104**, 065804 (2021).
[57] A. L. Watts and S. Reddy, Mon. Not. R. Astron. Soc. **379**, L63 (2007).
[58] A. I. Chugunov, Mon. Not. R. Astron. Soc. **371**, 363 (2006).
[59] A. G. Suvorov, H.-J. Kuan, and K. D. Kokkotas, Astron. Astrophys. **664**, A177 (2022).
[60] E. F. Brown, Astrophys. J. **531**, 988 (2000).
[61] A. Y. Potekhin and G. Chabrier, Astron. Astrophys. Rev. **645**, A102 (2021).
[62] N. K. Glendenning and F. Weber, Astrophys. J. **400**, 647 (1992).
[63] B. Haskell and A. Sedrakian, Astrophys. Space Sci. Libr. **457**, 401 (2018).